High-density microwell arrays enable controlled pseudoislet engineering for diabetes cell therapy

Biomedical Materials

PAPER

OPEN ACCESS

RECEIVED
9 March 2026

REVISED
11 June 2026

ACCEPTED FOR PUBLICATION
9 July 2026

PUBLISHED
30 July 2026

High-density microwell arrays enable controlled pseudoislet engineering for diabetes cell therapy

Charline Rosenberger[1,5,6,9], **Carolin Heller**[1,5,6,9], **Tomasz M Basiewicz**[4], **Susann Lehmann**[1,5,6], **Victoria Sarangova**[1,2], **Hany Abdelgawad**[1,5,6], **Undine Schubert**[1,5,6], **Janine Schmid**[1,5,6], **Carsten Werner**[2,3,8], **Stefan R Bornstein**[1,3,5,6,7], **Petra B Welzel**[2,10] **and Barbara Ludwig**[1,3,5,6,10,*]

[1] Department of Medicine III, University Hospital Carl Gustav Carus, Fetscherstraße 74, 01307 Dresden, Germany
[2] Division Polymer Biomaterials Science, Leibniz-Institut für Polymerforschung Dresden e.V., Hohe Str. 6, 01069 Dresden, Germany
[3] Center for Regenerative Therapies Dresden, Technische Universität Dresden, Fetscherstraße 105, 01307 Dresden, Germany
[4] Microstructure Core Facility, Center for Molecular and Cellular Bioengineering Technology Platform, Technische Universität Dresden, Tatzberg 41, 01307 Dresden, Germany
[5] German Center for Diabetes Research, Ingolstädter Landstraße 1, 85764 München-Neuherberg, Germany
[6] Paul Langerhans Institute Dresden of the Helmholtz Zentrum München at the University Clinic Carl Gustav Carus of Technische Universität Dresden, Helmholtz Zentrum München, Neuherberg, Germany
[7] Division of Diabetes & Nutritional Sciences, Faculty of Life Sciences & Medicine, King's College London, London SE1 1UL, United Kingdom
[8] Cluster of Excellence Physics of Life and Faculty of Chemistry and Food Chemistry, Technische Universität Dresden, Fetscherstraße 105, 01307 Dresden, Germany
[9] These authors contributed equally to this work as first authors.
[10] These authors contributed as senior authors.
[*] Author to whom any correspondence should be addressed.

E-mail: barbara.ludwig@ukdd.de, charline.rosenberger@ukdd.de, carolin.heller@ukdd.de and welzel@ipfdd.de

Keywords: macroencapsulation, pseudoislets, high-density microwell array, concave microwell, islet clustering, microarrangement, diabetes

Supplementary material for this article is available online

Abstract

Macroencapsulation systems for pancreatic islet delivery are an emerging strategy for cell replacement therapy in type 1 diabetes, aimed at eliminating systemic immunosuppression and enabling the use of alternative cell sources. A critical design challenge is to achieve high packing densities while maintaining sufficient oxygen and nutrient supply to ensure islet viability and function. This design-focused study presents a one-step method for the simultaneous and defined formation and spatial arrangement of uniformly sized pancreatic pseudoislets using high-density concave microwell arrays with potential for future integration into macroencapsulation devices. Microwells with diameters between 130 and 200 μm were arranged in a hexagonal pattern with inter-well spacings of 50 or 100 μm to maximize the packing density while maintaining separation between clusters. The effects of microwell depth, diameter, and inter-well spacing on pseudoislet size, morphology, viability, and glucose-stimulated insulin secretion were systematically evaluated using reaggregated rat islet cells as a standardized and well-characterized model system under normoxic and hypoxic conditions. The optimized microwell configuration enabled efficient pseudoislet formation with a tailorable, uniform size, high viability, and preserved insulin secretory function, even at high densities. This scalable microwell array technology addresses key limitations of current pseudoislet culture and transplantation methods, thus providing a base for improved macroencapsulation device design in diabetes cell therapy.

1. Introduction

Type 1 diabetes (T1D) is characterized by autoimmune-mediated destruction of insulin-producing beta-cells. The management and treatment of this chronic disease is challenging. Beta-cell replacement has been proven to successfully provide a functional cure for patients; however, it is limited by donor organ shortage and the need for persistent potent immunosuppression. Encapsulation of

pancreatic endocrine cells of xenogeneic or stem cell origin is an promising approach to treat T1D and may reduce or eliminate the need for immunosuppression [1–3].

Macroencapsulation systems designed for beta-cell replacement integrate the entire cell volume within a single container or scaffold, enabling straightforward procedures for both transplantation and retrieval. Immunoisolating encapsulation systems depend solely on diffusion for the exchange of molecules essential for cell function and viability [4]. The positioning of islet clusters within these implants is critical for optimal cell function. In encapsulation devices, insufficient separation or random arrangement of islet clusters can lead to aggregation or restricted and uneven nutrient and oxygen supplies, ultimately impairing cell viability and function [5]. In many previously reported macroencapsulation devices, for example, the TheraCyte^{TM} device (TheraCyte Inc.), the Islet Sheet (Cerco Medical LLC), the βAir (Beta O_2), the EnCRT (Encellin Inc.), and the PEC-Encap^{TM} device (ViaCyte Inc.), physical separation of the islets is not sufficiently implemented (figure 1(a)) [6–10]. The formation of a monolayer of evenly sized and spatially separated islets can improve their supply with oxygen and nutrients [4]. Macroencapsulation systems with intracapsular microstructures are expected to have a positive effect on both the functionality of the encapsulated cells and the encapsulation efficiency [11]. In fact, some micropatterned device systems have demonstrated promising preclinical outcomes with native islets, pseudoislets, and other cell types [12–14]. Particularly, concave microwells provide the advantage of creating uniformly sized islets below 200 µm [15].

Microwell array-based systems could enable uniform distribution of islets, ensuring a sufficient oxygen and nutrient supply to each islet throughout the device and minimizing the size of the device (figure 1(b)). Therefore, the optimal islet size and spacing are critical factors in the design of macroencapsulation devices. Although dense packing leads to competition for oxygen between islets, maximizing packing density remains essential for clinical translation. An optimal design for sufficient oxygen delivery minimizes the distance between islet clusters and the device surface to ensure the proximity of the islets to the surrounding vasculature [4]. Furthermore, the size of islet clusters is critical, as it affects oxygen diffusion to the inner cells, where insufficient oxygenation can lead to beta-cell dysfunction, apoptosis, and central necrosis. Large native islets with diameters of up to 500 µm are particularly affected by hypoxia due to the loss of their natural capillary network during the isolation process [16–18]. For this reason, small, uniform pseudoislets are used, which offer improved functionality and viability compared to larger native islets [19]. These pseudoislets can be generated by reaggregation of dissociated islet cells of different species (e.g. rodents, pigs, and humans) or from stem cell-derived endocrine cells. The size and composition of pseudoislets can be precisely controlled by adjusting factors such as the number of seeded cells per microwell, culture techniques, and the media used. However, the material and geometry of the microwells are critical to ensure the reliable and reproducible generation of small and robust pseudoislets.

Several materials have been reported as suitable for the fabrication of microwell arrays, including natural and synthetic polymers such as agarose, polyester, polyurethane, poly(ethylene glycol) (PEG), and poly(dimethylsiloxane) (PDMS) [20–26]. Combinations of polymers like poly(ether sulfone) (PES)—polyvinyl pyrrolidone (PVP) or poly(ethylene oxide terephthalate) (PEOT)—poly(butylene terephthalate) (PBT) have also been used to develop thin (porous) polymer films patterned with microwells [12, 27, 28]. Especially, PDMS microwells have been successfully applied to culture various cell types, including human native islets or pseudoislets, making them a popular choice owing to their favorable properties [15, 25, 29–31]. A key advantage of PDMS is its high oxygen permeability, which enhances oxygen diffusion to cells. This property makes it well-suited for microwell arrays designed to mitigate hypoxia and support cell viability and function in three-dimensional cultures [15]. PDMS further offers other benefits, including low material costs, straightforward curing from a prepolymer, biocompatibility, mechanical flexibility, and resistance to corrosion and ultraviolet (UV) light [32–42]. However, PDMS has a major drawback in cell biology: its pronounced surface hydrophobicity with a water contact angle of $\sim 108° \pm 7°$ [43, 44]. This leads to poor wettability by aqueous solutions, gas bubble formation in small cavities, and reduced efficiency of cell seeding. Hydrophobic surfaces can also adsorb biomolecules or small non-specific molecules from the culture medium or secreted by cells. Several strategies can be utilized to increase the hydrophilicity of PDMS, including plasma treatment, application of nonionic triblock copolymers (e.g. Pluronic® F-127), coating with charged molecules such as poly-L-lysine, or deposition of extracellular matrix proteins [43, 45, 46].

Polymer-based microwell arrays offer precise control over the well geometry enabled by photo- and soft-lithographic fabrication techniques [47, 48], yet their potential for creating small, closely packed wells tailored to islet-sized clusters has not been fully realized [12, 15, 23, 25, 26, 29, 30, 49–54]. A comparative analysis of the packaging density of microwell arrays reported in selected previous publications highlights the range of microwell diameters and inter-well spacings (defined here as the edge-to-edge distance between adjacent wells) used to date

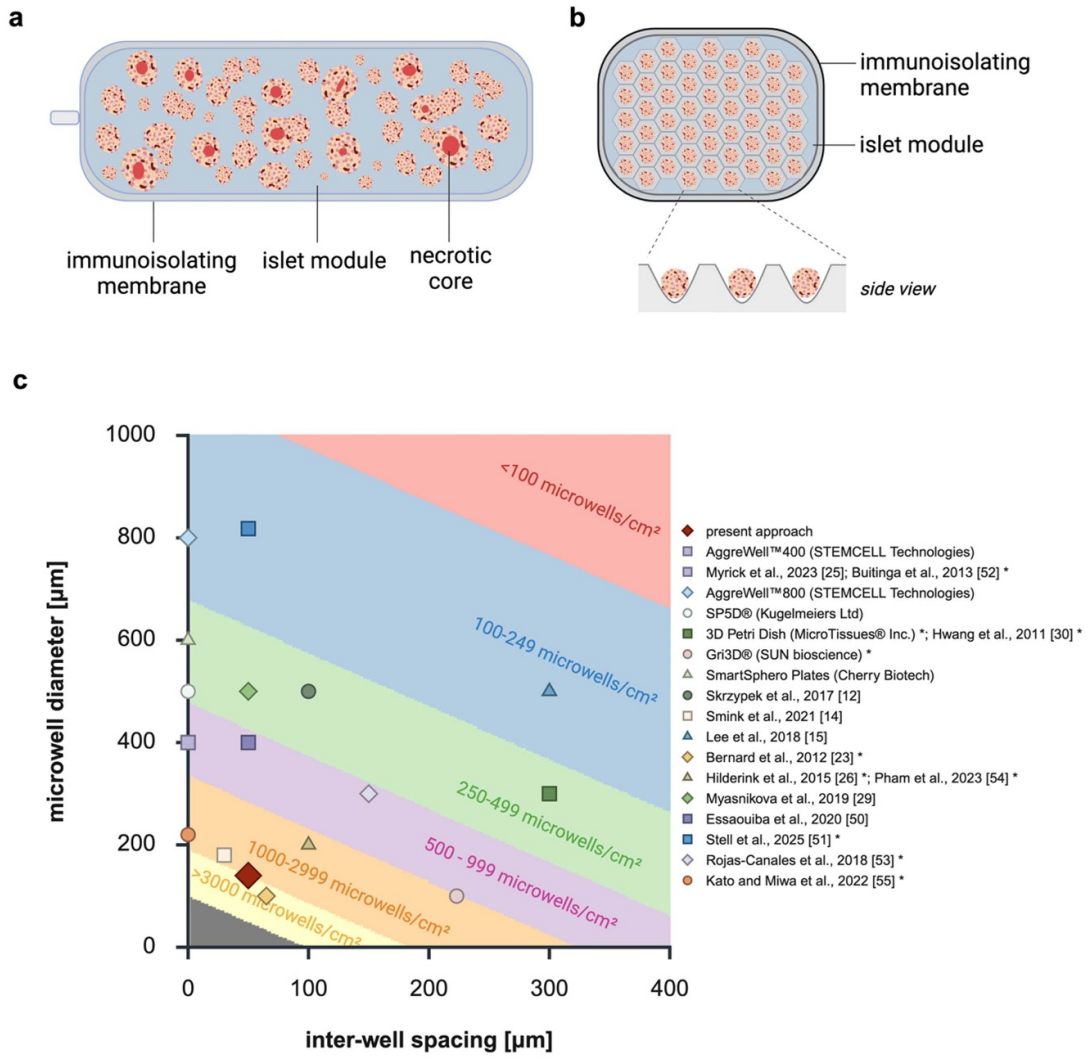

Figure 1. Pancreatic islet arrangement in macroencapsulation devices and microwell array configurations for pseudoislet formation. (a): Heterogenous native islet preparations and random islet placement without physical separation cause islet aggregation, restricted oxygen diffusion, and necrotic islet cores. (b): Concept of optimized islet microarrangement for high-density encapsulation of size-defined pseudoislets in a hexagonal pattern to prevent aggregation, optimize diffusion, and enhance islet survival and function. (c): Comparative overview of microwell dimensions (diameters and inter-well spacings, defined here as the edge-to-edge distance between adjacent wells) reported in selected studies. The high-density microwell array presented in this study represents the smallest known configuration that supports the formation of size-homogeneous pseudoislets by single-cell reaggregation within microwells. In studies where spacing was not explicitly reported, an estimate was taken from images provided in the original publications (indicated by *). If multiple sizes were reported, the smallest diameter above 100 µm was selected for inclusion in the plot. Estimated number of hexagonally packed microwells per cm^2 as a function of microwell diameter (D in µm) and inter-well spacing (d in µm). The calculation is based on the formula: hexagons per $cm^2 = 100 \times [(\sqrt{3}/2) \times ((D + d)/1000)^2]^{-1}$. An inter-well spacing of 0 indicates directly adjoining microwells without any gap. Background colors indicate different microwell packaging densities. Detailed data are presented in supporting information table S1. *Created with BioRender.com*

(figure 1(c)). Although previous studies have proposed and optimized microwell designs to achieve high packing densities for pancreatic islet culture, many of these approaches have limitations, such as inefficient seeding strategies, insufficient microwell depth for the formation of pseudoislets in the 100–150 µm size range, or the use of square-packed arrays that inherently limit maximum density. In this study, we address a critical gap in islet engineering, specifically the lack of systematically optimized microwell configurations for high-density, size-homogeneous pseudoislet formation, by designing and testing various PDMS-based array configurations differing in depth, diameter, and inter-well spacing. To the best of our knowledge, the systems developed here represent the smallest-scale microwell array configuration designed to support single-cell reaggregation into functional pseudoislets while ensuring their homogeneous distribution. To further enhance cell aggregation and uniformity, the wells were engineered with concave bottoms and arranged in a hexagonal layout, thereby promoting spherical pseudoislet formation

while maximizing the packing density. Importantly, this readily adaptable microwell array not only supports robust *in vitro* functions but is intended for future integration into macroencapsulation devices, providing a basis for a scalable and clinically relevant platform. Experiments were carried out using rat pseudoislets cultured under normoxic (20% oxygen) conditions, serving as a standardized and well-characterized *in vitro* model system. Furthermore, hypoxic culture conditions (5% oxygen) were investigated, with pseudoislets cultured for 67 h after the initial normoxic culture to mimic reduced oxygen tension in macroencapsulation or post-transplantation settings. Here, we present a geometrically optimized, transplantation-compatible high-density microwell platform that promotes efficient pseudoislet formation and dense cellular organization in a scalable format. This approach provides a foundation for preclinical *in vivo* evaluation across species and supports the development of tailored islet replacement therapies.

2. Results

2.1. Design of high-density microwell arrays for improved pseudoislet formation and maximized packing capacity

Hexagonally arranged, high-density microwell arrays with optimized microwell dimensions were developed to enable the generation of small pseudoislets and to ensure adequate oxygen and nutrient supply, while simultaneously maximizing packing density. To enable high islet densities of up to 3564 islets cm^{-2}, arrays were designed to feature small microwell diameters ranging from 130 to 200 μm with inter-well spacings of 50 or 100 μm (figure 2) for application within a macroencapsulation device. A commercially available microwell plate, Sphericalplate 5D® (SP5D®), was used as the control for cell culture experiments. This reference platform accommodates a maximum islet density of 480 islets cm^{-2} and features wells with a diameter of 500 μm and a depth of 320 μm.

To implement this design, a photolithography protocol was developed to fabricate SU-8 master molds with concave microwell bottoms, which served as patterned templates for PDMS double casting. The concave geometry was selected to promote efficient cell sedimentation and ensure consistent pseudoislet aggregation at the microwell bottom. The resulting PDMS surface morphology was visualized by scanning electron microscopy (figures 3(a)–(c)).

Two SU-8 masters (referred to as master 1 and master 2) were developed to investigate the effects of different microwell depths on pseudoislet formation and performance (figure 3(f)). The resulting PDMS microwell replicas matched the geometries of the corresponding SU-8 masters. Microwell depth was strongly dependent on the SU-8 master development, with SU-8 master 2 yielding significantly deeper microwells compared to SU-8 master 1 across all arrays ($p < 0.0001$). Microwells generated from SU-8 master 1 had depths ranging from 139.4 to 160.7 μm, whereas those fabricated from SU-8 master 2, developed with extended development time, ranged from 218.3 to 270.2 μm. The effect of microwell depth on pseudoislet formation was investigated using dissociated rat islet cells. PDMS microwell arrays replicated from both SU-8 master templates enabled pseudoislet generation for all well diameters, with larger microwell diameters (e.g. 200 μm, figure 3(d)) yielding more reproducible results compared to smaller microwell diameters. This difference was particularly evident in the microwells with diameters below 150 μm. In 130 μm diameter microwells prepared from SU-8 master 1, single cells were observed to displace from the wells on day 1, with displacement increasing until day 3. In contrast, deeper microwells of PDMS replicas made from SU-8 master 2 prevented cell displacement and enabled reliable pseudoislet formation even in smaller microwells (figure 3(e)). All pseudoislets remained in their position within the 130 μm sized microwells during medium changes. Therefore, PDMS microwell replicas fabricated from SU-8 master 2 were used for subsequent experiments to investigate the impact of microwell diameter and inter-well spacing on the pseudoislet size, circularity, viability, and *in vitro* function. To address the challenges caused by PDMS hydrophobicity during pseudoislet seeding and cultivation, plasma treatment was applied, followed by incubation with 5% Pluronic® F-127 solution in phosphate-buffered saline (PBS). This treatment increased surface hydrophilicity and eliminated bubble entrapment in the microwells to facilitate homogenous seeding of single cells.

In addition to microwell depth, the microwell diameter of the PDMS replicas was also analyzed for the two SU-8 masters. No significant differences in microwell diameter were observed between SU-8 masters 1 and 2, except for the 200/100 μm array, with arrays derived from SU-8 master 2 showing diameters closer to the intended design values (supporting information, figures S1).

Inter-batch analysis of microwell diameter and depth showed generally consistent values across batches, with only minor batch-to-batch variability (supporting information figures, S3 and S5). For SU-8 master 1, greater variability in PDMS microwell diameter was observed between batches, including significant differences under specific conditions. In contrast, PDMS replicas from SU-8 master 2 showed more consistent microwell diameters across batches and more closely matched the intended dimensions (figure S3). Overall standard deviations were low across all conditions. Intra-array analysis revealed local variations within individual arrays of

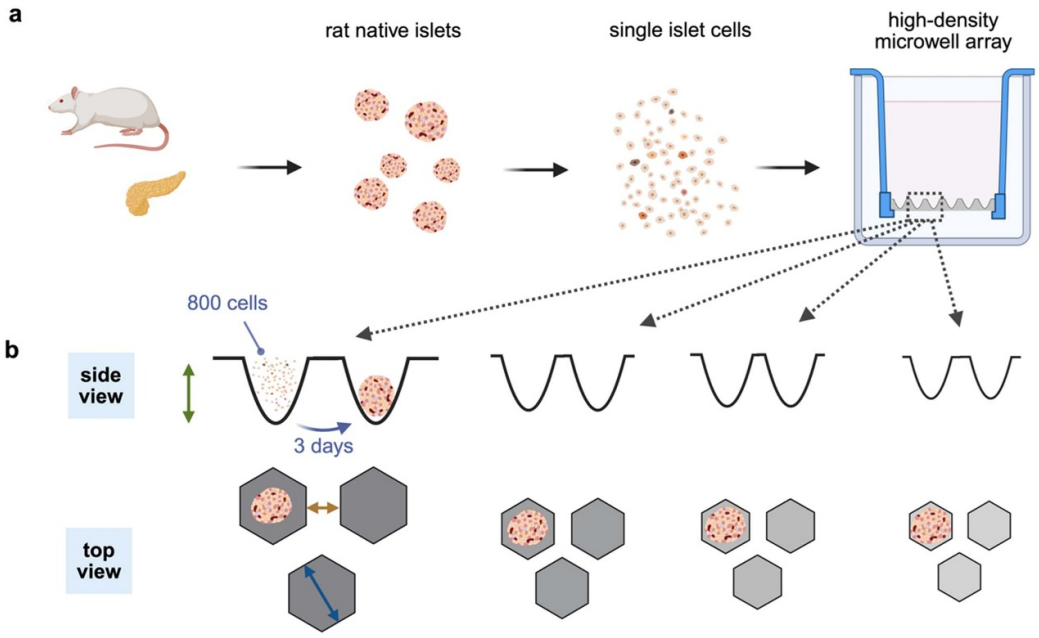

	200/100	150/50	140/50	130/50
depth [in µm] SU-8 master no. 1 and no. 2	161 and 270	144 and 230	139 and 230	140 and 218
diameter [in µm]	200	150	140	130
inter-well spacing [in µm]	100	50	50	50
microwell density hexagons / cm²	**1283**	**2887**	**3199**	**3564**

Figure 2. Design of high-density microwell arrays for microarrangement of pseudoislets. Featuring diameters of 130–200 µm in a hexagonal layout, these arrays efficiently distribute pseudoislets and maximize capacity. For clarity, the arrays are denoted using a diameter/spacing nomenclature (e.g. 200/100 indicates a microwell diameter of 200 µm with an inter-well spacing of 100 µm). (a): Method of seeding single islet cells into high-density microwell arrays. (b): Schematic side and top views of concave-bottom microwell structures with depths (green), diameter (blue), inter-well spacing (orange), and microwell density of the tested screening conditions. *Created with BioRender.com.*

a given batch, particularly for PDMS replicas from SU-8 master 1 and for master 2 in the 200/100 and 150/50 array designs, affecting both microwell diameter and depth (supporting information, figures S2 and S4).

2.2. Impact of microwell diameter and inter-well spacing on pseudoislet formation, viability and function

Microwell arrays with various diameters and inter-well spacings were screened to identify optimal parameters for preparing and culturing rat pseudoislets. A homogeneous distribution of pseudoislet clusters across the high-density microwell arrays was achieved for all tested microwell diameters when seeded with 600 cells per microwell (figure 4) and collected three days after seeding.

Comparing the mean sizes, the generated pseudoislets demonstrated a smaller size distribution than the native islets (134.5 µm ± 74.1 µm, $n = 3$) (figures 5(a) and (b)) as expected. While pseudoislets generated from 600 cells within commercial microwell cell culture plates (SP5D®) were 109.1 µm ± 19.3 µm ($n = 4$) in diameter, pseudoislets generated in custom-made microwell arrays of 150/50 and 130/50 measured 101.2 µm ± 19.4 µm ($n = 4$) and 103.3 µm ± 18.0 µm ($n = 4$), respectively. The size distribution of these pseudoislets remained within the predefined limits of ± 10 µm, as statistically tested for equivalence to the control condition SP5D® using two one-sided tests (TOST, see section 5.8; principle of equivalence test explained in supporting information figure S6). Similarly, pseudoislets cultured in 200/100 arrays (100.9 µm ± 29.7 µm, $n = 3$) and 140/50 arrays (100.5 µm ± 16.8 µm, $n = 4$) reached a comparable size, but did not demonstrate equivalence to SP5D® within the predefined boundaries. Comparing normoxic (20% O_2) and hypoxic (5% O_2) conditions, pseudoislets cultivated in the microwell array at hypoxic conditions showed a similar size in all tested microwell arrays (150/50: 99.9 µm ± 12.7 µm, $n = 3$; 140/50: 101.6 µm ± 19.8 µm, $n = 3$;

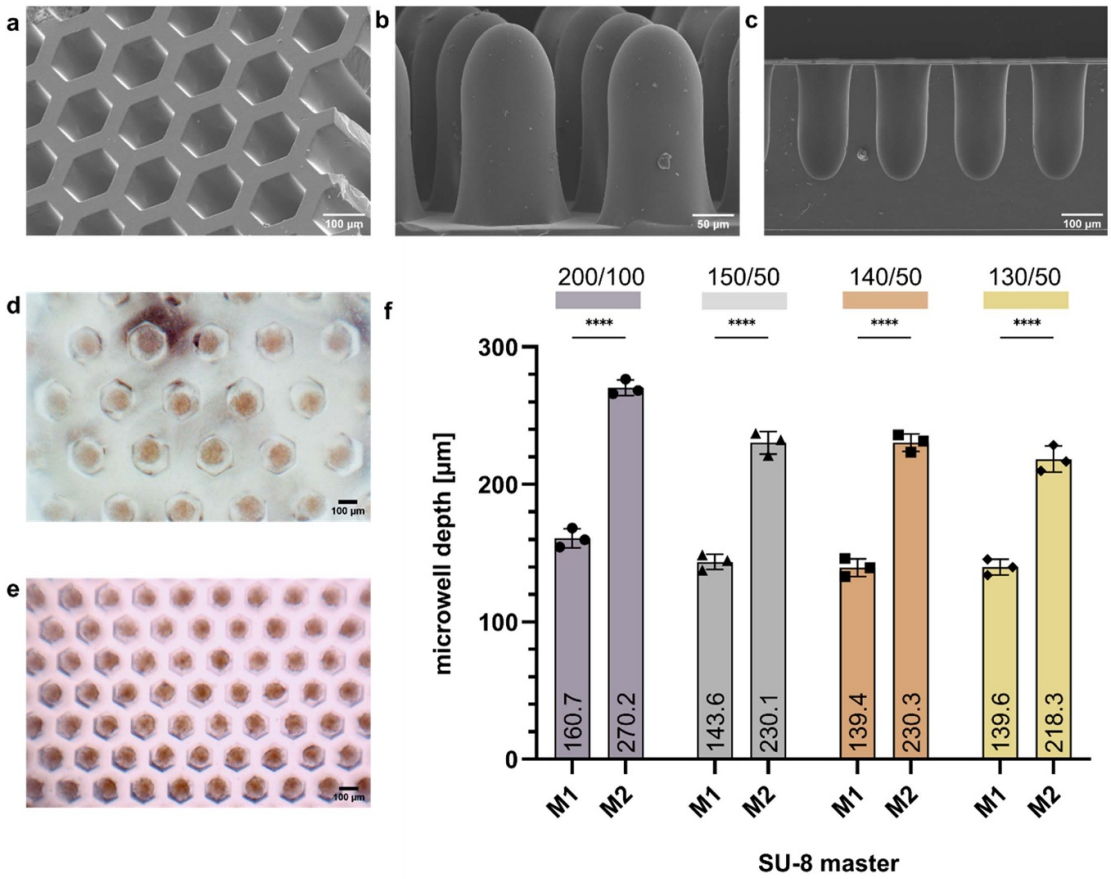

Figure 3. Concave microwell arrays, convex pillar replica structures, and optimization of microwell depth for pseudoislet seeding and culture. (a)–(c): Scanning electron microscopy images of PDMS microwell arrays replicated from SU-8 master 2 with increased depth: tilted top view of microwells (a), side view of the PDMS replica with convex pillars used for casting (b), and concave PDMS microwells in cross-sectional view (c). Dissociated rat islet single cells were seeded into the high-density microwell arrays at the same cell number per microwell and observed after three days of culture. (d): The pseudoislets formed in the microwell arrays with a diameter of 200 µm and an inter-well spacing of 100 µm (replicas of SU-8 master 1) had a uniform size distribution. (e): Deeper microwells obtained with SU-8 master 2 allowed successful pseudoislet formation within the small-diameter 130/50 microwell arrays. Brightfield images are shown (scale bar: 100 µm). (f): Characterization of the depths of PDMS microwell replicas generated from SU-8 masters 1 (M1) and 2 (M2). Depths were determined from cross-sectional images of microwell arrays at multiple positions from independent batches. Data are presented as mean ± SD ($n = 3$ batches; $N = 9$ measurements per batch; total $N = 27$). Statistical analysis was performed using a two-way ANOVA followed by Šídák's multiple comparisons test ($^{****}p < 0.0001$).

130/50: 97.1 µm ± 18.0 µm, $n = 3$) and were equivalent to those cultivated under normoxic conditions within the margin of 10 µm.

Circularity measurements of pseudoislets formed in high-density microwell arrays of 150/50 (0.68 ± 0.10, $n = 4$) and 130/50 (0.65 ± 0.11, $n = 4$) indicated values below 0.7, reflecting less rounded morphologies. In contrast, the pseudoislets cultured within the microwell arrays 200/100 ($n = 3$) and 140/50 ($n = 4$) showed a more uniform and rounded morphology with circularity values of 0.74 ± 0.09 and 0.72 ± 0.10, respectively. These circularity values were comparable to those observed for SP5D® plates (0.70 ± 0.10, $n = 4$) (figure 5(c)). Under hypoxia, the circularity of the pseudoislets formed in arrays of 140/50 (0.71 ± 0.09, $n = 3$) and 130/50 (0.66 ± 0.10, $n = 3$) were similar to those formed under normoxic conditions within a limit of ± 0.05. However, pseudoislets with improved circularity were achieved under hypoxia in the 150/50 microwell arrays (0.76 ± 0.08, $n = 3$).

The mean viability of the generated pseudoislets was greater than 77% for all groups (figure 6(b)). Within the predefined boundaries of ± 7.5%, the viability of native islets (88.1% ± 16.1%, $n = 3$), pseudoislets generated in 200/100 microwell arrays (85.4% ± 12.9%, $n = 3$) and 140/50 microwell arrays (85.7% ± 13.5%, $n = 4$) were comparable to those obtained using SP5D® plates (91.2% ± 12.8%, $n = 4$). However, the viability of the pseudoislets formed in the 150/50 microwell arrays (81.9% ± 19.4%, $n = 4$) and 130/50 microwell arrays (77.5% ± 19.0%, $n = 4$) was lower than that in the control condition (SP5D®) and did not demonstrate equivalence. Under hypoxic conditions, pseudoislets cultured in the 140/50 microwell arrays ($n = 3$) showed the highest viability (87.2% ± 11.9%). Similar results were observed for pseudoislets produced

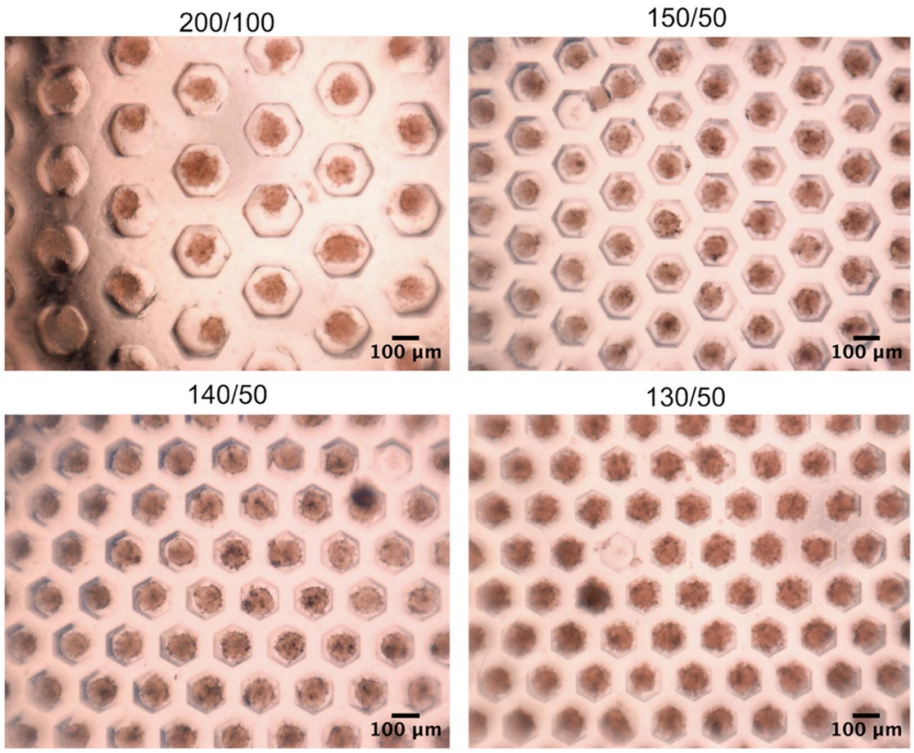

Figure 4. Formation and culture of rat pseudoislets in high-density microwell arrays with various diameters and inter-well spacings. Each microwell was seeded with 600 single cells and cultured for three days. Microwell dimensions are denoted as diameter/inter-well spacing (in µm). Brightfield microscopic images with a scale bar of 100 µm are shown.

in the 150/50 microwell arrays (85.4% ± 15.5%, $n = 3$). Clusters formed in microwell arrays of 130/50 (78.0% ± 14.6%, $n = 3$) showed the lowest viability under hypoxic conditions. All groups exposed to hypoxic conditions were equivalent to their respective normoxic conditions.

For all conditions, equally robust insulin secretion was observed, indicating comparable functional performance independent of the microwell array configuration. The *in vitro* function of the pseudoislets revealed no significant differences in basal or stimulated insulin secretion, as assessed using Dunn's multiple comparison test (figure 6(c)). No significant differences in insulin secretion were observed between pseudoislets formed and cultured in microwell arrays with identical microwell sizes under hypoxic and normoxic conditions. However, the 130/50 microwell array group exhibited higher basal insulin secretion than stimulated secretion, indicating a lack of a functional response under hypoxic conditions. Despite this, the pseudoislets generated in the other microwell array configurations maintained functional potency even in a low-oxygen environment.

2.3. Modeling oxygen distribution and consumption in pseudoislets cultured in microwell configurations of defined geometry

The oxygen distribution and consumption of microwell-cultured pseudoislets were investigated in a model considering three islets representatively with an islet size of 100 µm. The microwell diameter and inter-well spacing were selected to match the dimensions used in *in vitro* culture: microwells with diameters of 130 µm, 140 µm, and 150 µm were modeled with an inter-well spacing of 50 µm, whereas microwells with a diameter of 200 µm were modeled with a spacing of 100 µm. The spatial oxygen distribution within the high-density microwell arrays and islets was estimated using a 2D *in silico* model based on finite element modeling (FEM) of islet containing microwells. The chosen model dimensions provide a realistic *in vitro* representation of islet culture, as microwell systems generate uniformly sized pseudoislets and promote consistent experimental conditions.

During static culture, oxygen is supplied from both the medium-air interface and oxygen-permeable PDMS microwell bottom, creating a gradient as the islets consume oxygen. The closer the islets are arranged to each other, that is, the higher the islet density, the less oxygen is available, particularly at the islet core. The simulations indicate that islets in high-density microwell arrays experience an oxygen tension ranging from 0.0992 mol m^{-3} to 0.149 mol m^{-3} in the islet core when exposed to an oxygen concentration of 0.2 mol m^{-3} (equivalent to 20% oxygen at 37 °C) (figure 7). Microwell arrays with larger and wider spaced microwells (200/100) exhibited higher oxygen availability (0.131–0.151 mol m^{-3} or 13.1%–15.1% O_2 at 37 °C) than microwell arrays

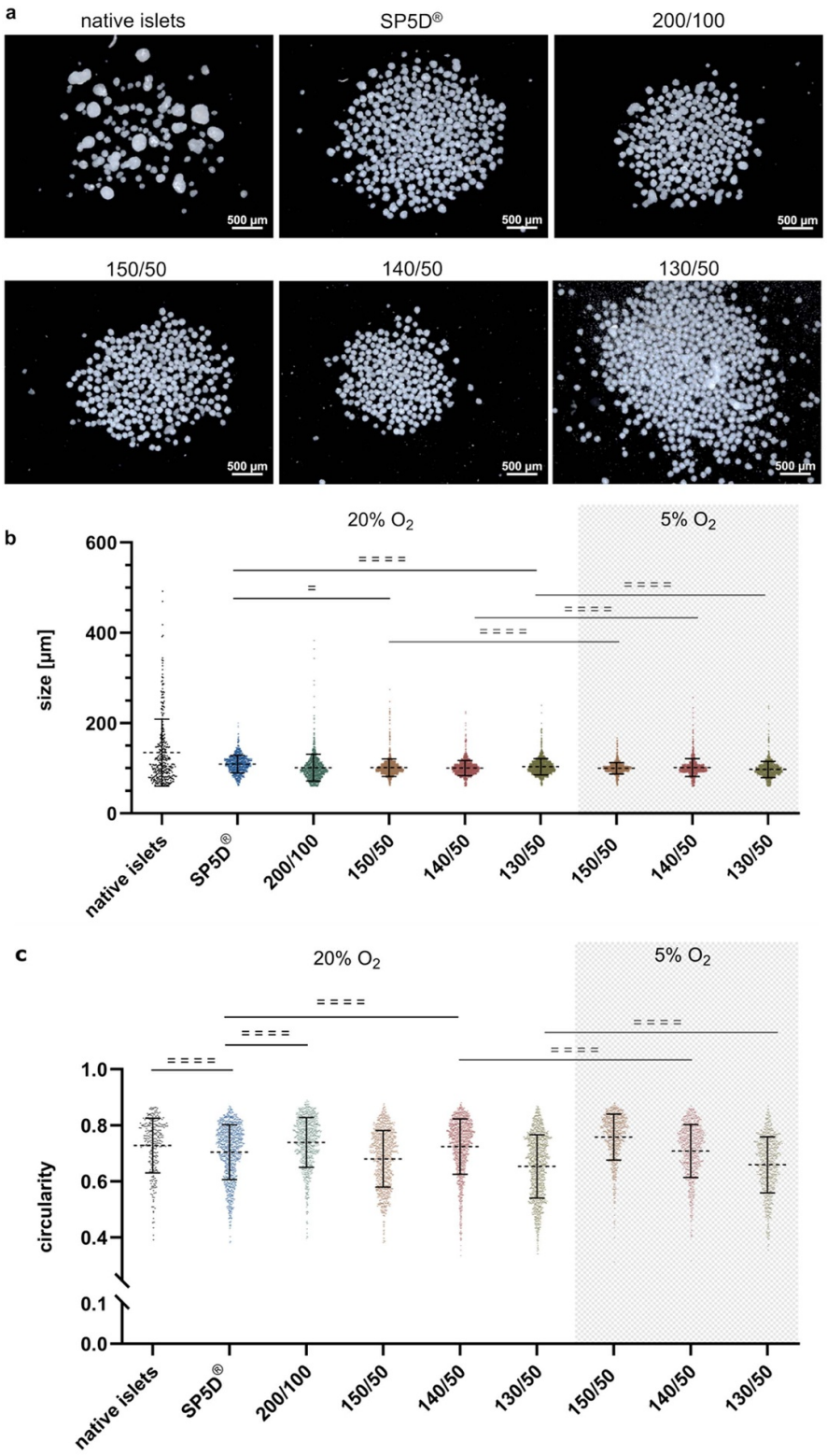

Figure 5. Morphology of rat pseudoislets clustered and cultured in high-density microwell arrays with various diameters and inter-well spacings under normoxic and hypoxic conditions. (a): Native islets and pseudoislets, collected from microwell arrays three days after seeding under normoxic conditions. Darkfield images (scale bar: 500 µm). (b): Size (in µm) and (c): circularity of native islets and pseudoislets. The scatter dot plot illustrates the data distribution, showing values with mean and standard deviation, based on three to four independent experiments with more than 100 analyzed islets per experiment under both normoxic and hypoxic conditions. For normoxia, an equivalence test (two one-sided tests) was performed with predefined lower and upper margins, comparing the pseudoislets generated in high-density microwell arrays to SP5D® pseudoislets. For hypoxia, pseudoislets were cultured for additional 67 h at 5% O_2. A two-sided equivalence test was applied within the same microwell array group comparing results to the normoxic conditions. ' = ' indicates equivalence of $p < 0.05$; '= = = = ' indicates equivalence of $p < 0.0001$.

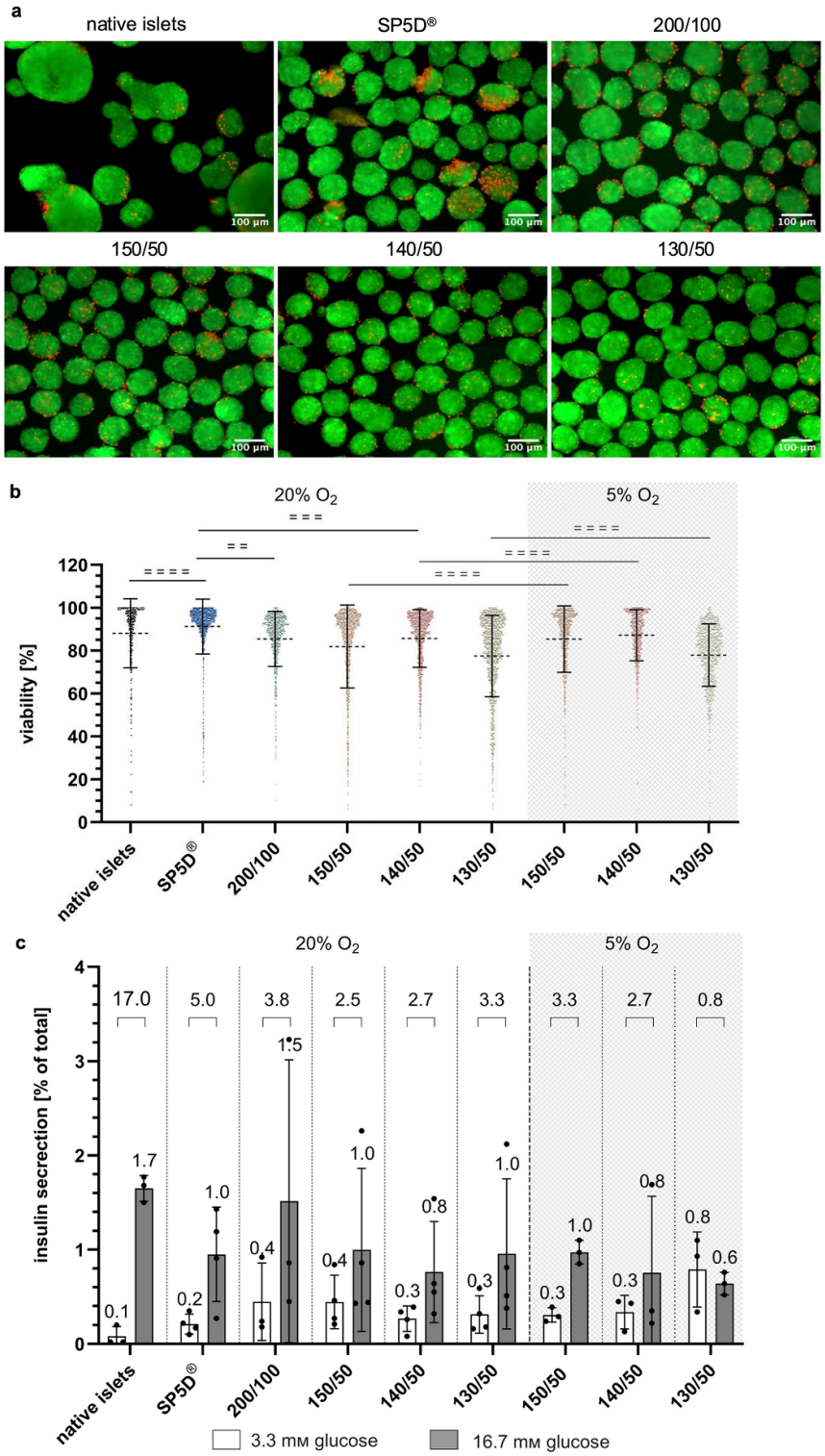

Figure 6. Viability and function of rat pseudoislets in high-density microwell arrays with various diameters and inter-well spacings under normoxic and hypoxic conditions. (a): Native islets and pseudoislets were collected after three days of cultivation under normoxic conditions. Live cells (green, fluorescein diacetate); dead cells (red, propidium iodide). Fluorescence images (scale bar: 100 µm). (b): Viability (in %) of native and pseudoislets. The scatter dot plot illustrates the data distribution, showing values with mean and standard deviation, based on three to four independent experiments with more than 100 analyzed islets per experiment under both normoxic and hypoxic conditions. For normoxia, an equivalence test (two one-sided tests) was performed with predefined lower and upper margins, comparing the high-density microwell arrays to pseudoislets cultured in commercial microwell plates. For hypoxia, pseudoislets were cultured for additional 67 h. A two-sided equivalence test was applied within the same microwell array group, comparing results to the normoxic conditions. '= =' indicates equivalence of $p < 0.01$; '= = =' indicates equivalence of $p < 0.001$; '= = = =' indicates equivalence of $p < 0.0001$. (c): Functionality (static GSIS) of native islets and pseudoislets. Data represent the mean ± standard deviation of three to four individual experiments. The stimulation index of each sample is represented above each corresponding group. A Kruskal–Wallis test followed by Dunn's multiple comparison was performed to compare the basal (white, 3.3 mM glucose) and stimulated (gray, 16.7 mM glucose) insulin secretion values of the SP5D® group with those of the other groups. A Student's *t*-test was used to compare the basal and stimulated insulin secretion between the different oxygen conditions (20% and 5%) for each microwell size.

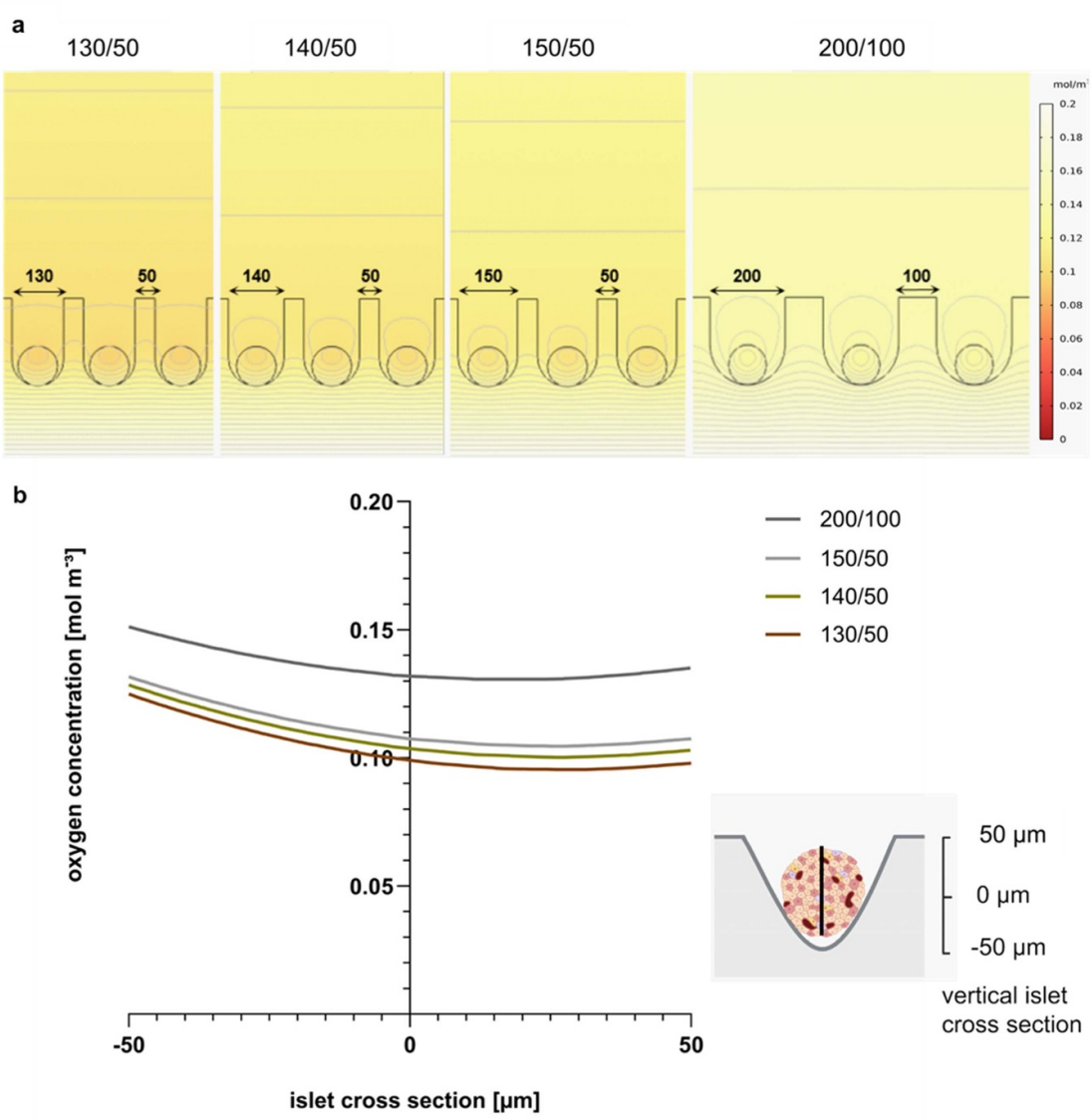

Figure 7. Simulated spatial oxygen concentration within and around pseudoislets cultured in high-density microwell arrays. (a): FEM simulation of the oxygen gradient under static conditions. (b): Oxygen concentration at the vertical cross section of an islet. *Created with BioRender.com.*

with smaller and denser spaced microwells (150/50, 140/50, and 130/50) (0.095–0.131 mol m^{-3} or 9.5%–13.1% O_2 at 37 °C). The lowest oxygen concentration of 0.0954 mol m^{-3} was obtained by these simulations for islets in 130/50 high-density microwell arrays at a vertical islet cross section of 29 µm.

3. Discussion

Transplantation of pancreatic islets within encapsulation-based systems represents a promising therapeutic approach for T1D. In current approaches, islets are typically introduced into encapsulation devices as a suspension of clusters or embedded in hydrogel matrices. However, these loading strategies often result in random spatial distribution and clustering, which reduces entrapment efficiency and limits uniform dispersion within the device [12, 14, 25, 27, 50, 52–55]. In addition, variability in islet cluster size further contributes to inhomogeneous device loading and inconsistent culture outcomes. Only a limited number of studies have addressed the challenge of achieving a homogeneous distribution of size-defined islets within macroencapsulation systems.

This study establishes a geometry-driven framework for balancing pseudoislet density and oxygen-dependent functionality under diffusion-limited conditions. To address the limitations of current loading strategies, high-density microwell arrays were employed as structured platform for the controlled formation and spatial organization of pseudoislets. By seeding dissociated single islet cells into defined microwells, reproducible pseudoislet formation with uniform size and precise positioning was achieved.

A central finding of this study is that high-density microwell arrays, defined by diameter, inter-well spacing, and depth, preserve the viability and glucose-stimulated function of pseudoislets. While reducing inter-well spacing increases pseudoislet density, it simultaneously limits oxygen and nutrient availability, underscoring the need to balance packing density with functional stability for downstream applications. In many previously reported systems, microwell diameters and inter-well spacings are substantially larger than the size of individual islets [12, 15, 25, 26, 28–30, 50–55]. While this enhances oxygen availability around each cluster, it also necessitates larger dimensions to achieve therapeutically relevant cell numbers. Only a limited number of studies have explored microwell arrays with small diameters, reduced inter-well spacing, and depths tailored for pancreatic islet culture. For example, Bernard *et al,* Smink *et al,* and Shinohara *et al* reported comparatively compact microwell configurations; however, in these cases, the microwell depth appeared insufficient to reliably support the formation and culture of pseudoislets in the physiologically relevant size range of approximately 100–150 μm [14, 23, 56]. In addition, these approaches exhibit specific methodological differences. Smink *et al* employed concave microwells, but exclusively seeded native islets, thereby limiting control over spatial arrangement and increasing the risk of islet aggregation [14]. Bernard *et al* and Shinohara *et al* demonstrated cluster formation directly within microwells, enabling size control and homogeneity; however, the use of *ß*-cell lines limits the physiological relevance of their findings [14, 23]. In Bernard *et al* the square-packed arrangement restricts achievable packing density compared to hexagonal configurations [23]. Pham *et al* improved entrapment efficiency by distributing pseudoislets into microwells, but did not address high-density spatial organization within a defined geometric framework [54]. Together, these studies highlight that while key aspects such as pseudoislet formation, concave geometries, or loading strategies have been investigated individually, a systematic optimization of microwell geometry for high-density pseudoislet arrangement under diffusion-limited conditions has not yet been established. In contrast, the present study specifically targets smaller microwell geometries (130–200 μm diameter, 50 or 100 μm spacing) to maximize pseudoislet density within a confined space. This design strategy resulted in pseudoislet densities of up to 3564 islets cm^{-2} in the 130/50 configuration, representing a nearly seven-fold increase compared to the control condition, the commercial microwell culture plate SP5D® (480 islets cm^{-2}).

The controlled microarrangement of pseudoislets represents a key advantage of this approach. The hexagonal arrangement of concave microwells enables homogeneous distribution and spatial separation of uniformly sized pseudoislets, thereby preventing aggregation and reducing local competition for oxygen and nutrients. This is in contrast to randomly distributed or clustered islet configurations, which are associated with oxygen availability and increased risk of necrosis. The resulting single-layer organization is particularly relevant for macroencapsulation systems, where minimizing diffusion distances to the surrounding vasculature is critical for both oxygen supply and insulin exchange. The pseudoislet approach further enables precise control of islet size by adjusting the number of seeded cells per microwell. Compared to native pancreatic islets, which often exhibit large size variability, this allows the generation of uniformly sized clusters, thereby reducing the risk of central hypoxia and necrosis and improving overall functional stability. To achieve controlled pseudoislet formation and long-term culture, both microwell geometry and material selection are critical design parameters. Previous studies have demonstrated, that polymer composition can influence islet function and cellular homeostasis [57]. PDMS is widely used due to its high oxygen permeability and general biocompatibility, supporting the cultivation of various cell types including pseudoislets [15, 31, 58, 59]. Certain material-related aspects of PDMS have been discussed in the literature in the context of extended culture durations, including potential effects associated with uncrosslinked oligomers, as well as gradual changes in surface and mechanical properties over prolonged time periods under specific conditions [60, 61]. In the present study, no indications of structural changes or instability of the PDMS microwell arrays were observed. However, for long-term applications, both material stability and potential effects on cellular behavior would require further investigation. From a functional perspective, cellular aggregation and the establishment of functional cell-cell contacts predominantly occur within the first days after seeding, thereby defining short-term culture as the critical window for evaluating structural and functional performance of the microwell array system. While extended culture periods may provide additional insights into long-term viability and function, this was beyond the scope of the present design-focused study and will be addressed in future investigations. In addition to material properties, microwell geometry plays a decisive role in supporting pseudoislet formation. Concave-bottom microwells promote uniform aggregation and improved functionality compared to flat geometries, consistent with previous reports [29, 30, 62]. For example, Hwang *et al* demonstrated that concave PDMS microwells facilitate the formation of uniformly sized pseudoislets with functional properties comparable to native islets, whereas flat-bottom geometries resulted in reduced insulin secretion [30]. These findings are in agreement with our results and further support

the importance of combining appropriate material properties with optimized geometric design.

Although optimization of microwell parameters was performed using rat islet cells, the underlying design principles, microwell diameter, inter-well spacing, and depth, are based on general biophysical considerations of cell aggregation and oxygen diffusion and are therefore expected to be broadly applicable across species. Nonetheless, species-specific differences in oxygen consumption may require minor adjustments in seeding density or culture conditions. Importantly, the microwell system can be readily adapted by modifying the SU-8 master molds, allowing systematic variation of geometric parameters. In particular, microwell depth represents a critical parameter, as it directly influences diffusion distances within confined environments. Reducing microwell depth minimizes the distance for oxygen and nutrients to reach the pseudoislets and support rapid glucose responsiveness, highlighting its importance for the design of high-density pseudoislet systems. Shallower microwells (139.4–160.7 μm) were less effective in retaining cells during the initial aggregation phase, leading to cell displacement, particularly in smaller diameter wells. In contrast, deeper microwells (218.3–270.2 μm) enabled reliable pseudoislet formation across all tested diameters, including 130 μm wells. These findings indicate that sufficient geometric confinement is required to support stable aggregation and reduced dimensions. Importantly, the increased depth achieved with SU-8 master 2 improved aggregation conditions while maintaining high reproducibility. Minor variations in microwell geometry are most likely attributable to PDMS curing-induced shrinkage and measurement limitations, but are not expected to affect pseudoislet formation or size distribution.

In addition to microwell depth, inter-well spacing and diameter constrain cell loading per microwell and thus the pseudoislet clustering and size, which may have implications for function. While all tested configurations supported pseudoislet formation with comparable viability and function under normoxic conditions, differences became apparent under hypoxic conditions. The 130/50 microwell array configuration exhibited impaired functionality, likely due to limited oxygen and nutrient diffusion in highly confined geometries. In contrast, the 140/50 microwell array configuration provided a favorable balance between high density and preserved function, identifying an optimal parameter range within the tested design space. The hypoxic culture condition (5% oxygen) applied in this study served as a functional stress test to evaluate geometry-dependent oxygen limitations relevant for macroencapsulation and early post-transplantation conditions. The combined assessment of viability and insulin secretion indicates preserved cellular survival and functional competence in the majority of configurations under hypoxic conditions, demonstrating that appropriate geometric design can mitigate oxygen limitations even at high pseudoislet densities. However, the observed functional impairment in the most compact configuration highlights the existence of a critical threshold beyond which diffusion limitations dominate. Additional analyses of cellular metabolism (e.g. ATP content), oxidative stress (e.g. reactive oxygen species), and apoptosis-related pathways (e.g. BAX/BCL-2 expression or Caspase-3 activation) could provide valuable insight into the mechanisms contributing to hypoxia-induced functional alterations of pseudoislets and represent an important subject for future research. To further interpret these findings in the context of oxygen transport, FEM was used to analyze oxygen diffusion within the microwell arrays. The simulations indicate that reduced inter-well spacing and increased packing density lead to steeper oxygen gradients and limited oxygen availability, particularly in the core regions of densely packed pseudoislets. These results are consistent with the experimentally observed reduction in functional performance in the most compact configurations, confirming that oxygen diffusion represents a key constraint at high densities. At the same time, the modeling supports the conclusion that appropriate geometric design can mitigate these limitations by maintaining diffusion distances within a critical range. These findings emphasize that both oxygen availability and spatial organization must be considered together when designing high-density pseudoislet systems. To further contextualize these findings, oxygen availability in islet culture systems has been extensively studied. Oxygen levels *in vivo* vary substantially across physiological compartments, with generally low oxygen tensions in most tissues [63–65]. Previous modeling and experimental studies have demonstrated that oxygen supply can be enhanced through diffusion via oxygen-permeable materials such as PDMS [15, 56]. For example Buchwald *et al* showed that dual oxygenation supply through medium and membrane can significantly improve oxygenation of the islets [66]. Similarly, Avgoustiniatos *et al* demonstrated increased oxygen availability at high cell densities using oxygen-permeable membranes [67]. In line with these findings, the PDMS-based microwell system used in this study supports oxygen diffusion from below, contributing to the maintained viability and function observed under hypoxic conditions. At the same time, literature reports confirm that oxygen gradients persist within islet cultures and *in vivo* environments, reinforcing the importance of minimizing diffusion distances through optimized spatial organization [68–70].

To estimate the translational relevance of the presented design, a theoretical scaling approach was applied. For a typical 70 kg patient requiring a dose of 5000 IEQ kg^{-1}, the 140/50 microwell array

configuration with a density of 3199 microwells cm^{-2} would correspond to an encapsulation surface area of approximately 350 cm^2. In a double-sided configuration, this would translate into a device radius of approximately 7.5 cm. While this calculation represents a simplified approximation, it highlights the importance of maximizing pseudoislet density through geometric optimization in order to achieve clinically relevant cell numbers within feasible device dimension. It is important to note that device integration was intentionally not addressed in the present study in order to isolate geometry-dependent effects on pseudoislet formation and function. Macroencapsulation involves additional device-level challenges, including membrane properties, diffusion distances of molecules, and host response such as fibrotic overgrowth, which are largely independent of pseudoislet microarrangement. The presented microwell arrays are designed as a modular platform for future integration into such systems.

Taken together, this study demonstrates that microwell geometry is a critical determinant of pseudoislet density, viability, and function under diffusion-limited conditions. By defining the design space for balancing packing density and oxygen-dependent functionality, the presented approach provides a foundation for the development of scalable and clinically relevant macroencapsulation strategies for diabetes therapy and informs the rational design of future macroencapsulation systems.

4. Conclusion

In the context of macroencapsulation strategies, the microarrangement of islet clusters is a crucial innovation. This approach aims to maximize the transplantable islet mass while maintaining islet survival and function, addressing a significant gap in many current macroencapsulation devices where such microarrangement is not the primary focus. The pseudoislet microwell array presented here enables integration of the maximum islet mass in a monolayer at the smallest area. To achieve this, hexagonally arranged microwells with varying diameters, interwell spacings, and depths were developed, providing a design that is expected to be broadly applicable. The results demonstrated that the viability and glucose-stimulated function of pseudoislets are not compromised by the high-density microwell arrangement. Furthermore, mimicking the low oxygen conditions that islets are often exposed to *in vivo*, did not reduce the function or viability of closely packed pseudoislets. Consequently, the proposed one-step generation and microarrangement strategy of small uniformly sized pseudoislets represents a scalable technology for application in macroencapsulation devices, thereby enhancing the prospects for effective T1D treatment. Future studies will first investigate the effects of integrating the microwell array into a macroencapsulation device under various oxygen culture conditions and subsequently evaluate the performance of the optimized design using human islets or xenogeneic sources, such as porcine pancreata. Minor adjustments in geometry or cell seeding density may be required for different species or alternative cell sources and can be readily implemented by modifying the SU-8 master, thereby highlighting the flexibility of the presented approach. These efforts aim to facilitate the successful translation of this technology into clinical practice, including *in vivo* biocompatibility testing.

5. Materials and methods

5.1. Fabrication and characterization of high-density microwell arrays

SU-8 masters were fabricated using photolithographic techniques. Briefly, silicon wafers (Microchemicals GmbH) were spin-coated with a negative epoxy-based SU-8 2075 photoresist (Kayaku Advanced Materials, Inc.) and exposed to UV light through a brightfield photomask (JD Photo Data) using an EVG 620 mask aligner (EV Group GmbH). The photomask contained the desired microwell patterns, which were designed using K-Layout. After the post-exposure bake, the unexposed regions were partially removed by immersion in a developer (mr-Dev 600, Microresist Technology GmbH). The depth of the microwells was controlled by adjusting the development time of the fabricated masters. Concave microwells were created by thermally reflowing the photoresist. Subsequent flood exposure and final baking fully crosslinked the previously unexposed regions of the photoresist, forming microwell structures [71, 72]. SU-8 masters were functionalized using 1 H, 1 H, 2 H, 2 H-Perfluorooctyltriethoxysilane (Apollo Scientific) [73].

High-density microwell PDMS arrays were fabricated by replicating the SU-8 master using soft lithography techniques. To this end, PDMS base (SYLGARD™ 184 Silicone Elastomer Base, DOW®) was mixed in a ratio of 1:10 with the corresponding curing agent (SYLGARD™ 184 Silicone Elastomer Curing Agent, DOW®). Air bubbles formed during the mixing process and poured onto the SU-8 master were removed by applying vacuum. The PDMS was then polymerized at 78 °C for 2.5 h. The cured PDMS negative replica, featuring convex pillars, was carefully peeled off from the SU-8 master. Finally, microwell arrays were replicated from the convex pillars after plasma-treating the surface with oxygen plasma for 120 s at 50 W (Tucano Plasma System, Gambetti Kenologia Srl) and immersing the structures in a surfactant solution (1:300). Circles of the

microwell arrays were then punched out using a 5 mm biopsy needle. These PDMS sections were then affixed with a silicone adhesive (DOWSIL™ SE 1700, DOW®) into 3D-printed structures made of BioMed Clear resin (Formlabs GmbH) using a Form 3B+ 3D Printer [74]. The adhesive was cured at 78 °C for at least 2.5 h. On the day before the experiment, the microwell arrays were disinfected with 70% isopropyl alcohol for at least 15 min. The dried microwell arrays were treated with oxygen plasma for 120 s at 50 W and immediately immersed in 5% Pluronic® F-127 (Sigma-Aldrich®) for 20 min. The fabricated microwell arrays were stored in PBS (Sigma-Aldrich®).

Three independent PDMS microwell array batches were replicated from the corresponding SU-8 master to assess the reproducibility of microwell fabrication. Microwell diameters were quantified from top-view images and microwell depths from cross-sectional images across three independent PDMS batches fabricated from the SU-8 masters 1 and 2 using an Axio Scope. A1 fluorescence zoom microscope (Carl Zeiss Microscopy Germany GmbH). Intra-array variability was evaluated by measuring the size of multiple PDMS microwells across different regions of the same PDMS array batch, whereas inter-batch variability was evaluated between different PDMS array batches. PDMS microwell arrays and negative replicas were analyzed by scanning electron microscopy using an ESEM Quattro (Thermo Fisher Scientific Inc.) in HiVac mode at an acceleration voltage of 10kV. Prior to imaging, the samples were sputter-coated with gold.

The following microwell diameters and inter-well spacings were chosen for the experiments: (1) 200/100, (2) 150/50, (3) 140/50, and (4) 130/50. In this notation, the first value denotes the microwell diameter and the second denotes the inter-well spacing. The influence of microwell depth derived from the two SU-8 masters on the formation and cultivation success of rat pseudoislets was investigated.

5.2. Isolation of rat islets

All animal studies were conducted with the approval of the local animal care committee (Saxony, Germany) in accordance with institutional guidelines and national animal welfare legislation (license numbers TV T 2/2018 and TV T 4/2023). The animals were housed under standard conditions for at least one week before the experiments. Pancreatic islets were isolated from 14 to 16 week old female Wistar rats (Janvier Laboratory, Le Genes St Isle, France), as previously described [75]. The pancreata were digested with collagenase (from *Clostridium histolyticum*, 1 mg ml^{-1}, Sigma-Aldrich®)/DNAse solution (0.1 mg ml^{-1}, Roche Deutschland Holding GmbH) in RPMI 1640 medium (Gibco™), and islets were purified using Ficoll (Cytiva) density gradient centrifugation (1.125 g cm^{-3},1.096 g cm^{-3}, 1.08 g cm^{-3} and 1.069 g cm^{-3}). After isolation, islets were cultured overnight in RPMI 1640 medium supplemented with 10% fetal bovine serum (FBS, Gibco™), 5.5 mM glucose (Sigma-Aldrich®), 10 mM HEPES buffer (Sigma-Aldrich®), 1% penicillin, and streptomycin (10.000 U ml^{-1}, Gibco™) at 37 °C and 5% CO_2.

5.3. Formation and cultivation of pseudoislets in microwell arrays with different configurations

Prior to cell culture, the microwell arrays were washed with PBS and medium, and sterilized by UV treatment for 30 min. Exocrine tissue was manually removed from the native islet preparation. After two washes with PBS, native islets were digested into single cells using 1X TrypLE™ Express Enzyme (Thermo Fisher Scientific Inc.) for at least 12 min at 37 °C, as previously described [26]. Cells were seeded at a density of 600 cells per concave microwell into microwell arrays of different configurations and a commercially available microwell plate (SP5D®, Kugelmeiers Ltd). Single cells were settled into the microwell arrays by centrifugation using the Heraeus™ Multifuge™ X3R (Thermo Scientific™) at 100 g, applying a soft acceleration (ACC) and deceleration (DCC) setting of 6/6 for 1 min.

Native islets and pseudoislets were maintained at 37 °C in a humidified incubator at 5% CO_2. Initially, all samples were cultured in an incubator set to 20% O_2 for three days. Pseudoislets in microwell array configurations 150/50, 140/50, and 130/50 were prepared in duplicate. Native islets and pseudoislets cultured in SP5D® plates were cultured in parallel as controls. The SP5D® system was used as a reference platform for pseudoislet formation, as it represents an established and widely used microwell-based culture system with reproducible and standardized culture conditions. It served as a functional benchmark for comparison with the customized microwell arrays. To mimic the typical hypoxic conditions at the graft site early after device implantation, these duplicates were transferred to a hypoxic incubator set to 5% O_2 for an additional 67 h. The medium was changed every 1–2 d during the culture period.

5.4. Glucose-stimulated insulin secretion (GSIS)

To assess islet functionality, a static GSIS test was performed. Three technical replicates were performed for each experiment, with each replicate consisting of 40 hand-picked pseudoislets transferred to cell strainers (pluriStrainer Mini 5 or 10 µm, pluriSelect Life Science UG & Co.KG). The cells were washed and preincubated for 2 h at 37 °C in Dulbecco's Modified Eagle's medium (DMEM, Gibco™) supplemented with 0.5% protease- and fatty acid-free bovine serum albumin (BSA, Sigma-Aldrich®), 2 mM glutamine (Gibco™), 10 mM HEPES buffer and 3.3 mM glucose (basal media). After the pre-incubation step, the inserts were transferred into fresh basal media (1 ml) for 60 min, followed by incubation in stimulatory

Table 1. Lower and upper bound in the equivalence testing to the SP5D® group.

	Lower equivalence bound	Upper equivalence bound
Viability	−7.5%	+7.5%
Size	−10 μm	+10 μm
Circularity	−0.05	+0.05

media (DMEM 16.7 mM glucose) for an additional 60 min. At the end of each time point, the medium was collected and frozen at −20 °C for further analysis. Radioimmunoprecipitation assay buffer (Sigma-Aldrich®) was used to extract total insulin.

5.5. Insulin measurement by homogeneous time-resolved fluorescence assay (HTRF)

Insulin content was quantified using an Insulin Ultra-Sensitive HTRF kit (Cisbio) according to the manufacturer's instructions, and the resulting fluorescence was measured using a BIOTEK fluorescent reader (excitation/emission wavelengths of 620/665 nm). Each value was normalized to the total insulin content. The stimulation index was calculated as the ratio of insulin secreted at high glucose concentrations to insulin secreted at low glucose concentrations.

5.6. Viability staining

The viability of the pseudoislets was determined by fluorescein diacetate (FDA) and propidium iodide (PI) (Sigma-Aldrich®) staining after cultivation. FDA (5 mg ml^{-1} in acetone) was diluted 1:100 with PBS. Pseudoislets were transferred into a small volume of culture medium, and fluorescent dyes were added at a 1:10 ratio to a final concentration of 5 μg ml^{-1} FDA and 100 μg ml^{-1} PI. Fluorescence microscopy was performed using an Axio Scope. A1 fluorescence zoom microscope (ZEISS).

5.7. Image analysis

Data evaluation for fluorescence microscopy analysis was performed using an in-house Fiji macro script. A minimum of 100 islets were analyzed to determine their viability, Feret diameter, and circularity. Viability was defined as the ratio of the stained red area (PI, dead cells) to the total cell area (live and dead cells). Another key parameter evaluated was islet circularity, which provides information about the overall spherical shape of the islets. Circularity values ranged from 0 to 1, with higher values indicating a more spherical shape.

5.8. Statistical analysis

Relevant statistical tests, sample sizes, and p-values are presented in the corresponding figures. Data are presented as scatter-dot plots with the mean ± standard deviation. The spheroids clustered in the microwell arrays and native islets were tested for equivalence to SP5D® pseudoislets by selecting an experimentally relevant boundary below and above the mean (table 1, figure S6). In the equivalence test, p-values were calculated using TOST for normally distributed (Gaussian distribution) means and corrected p-values using the Holm–Bonferroni method [76, 77]. For non-normally distributed means (GSIS data), Kruskal-Wallis test followed by Dunn's multiple comparison test was used to compare the experimental groups to the commercial microwell plate.

To evaluate culture conditions under hypoxia, an equivalence test with the same pre-defined margins for the parameter size, circularity, and viability was performed to compare the two experimental groups, 20% and 5% O_2. The Student's t-test was used to evaluate the non-normally distributed means of the GSIS data. Differences between conditions were considered significant at $p < 0.05$ (*), whereas equivalence was denoted with an equal sign (=) for $p < 0.05$. Statistical analyses were performed using R (version 2024.04.1 + 748, Posit Software, PBC). Graphs were constructed using Prism 9 (GraphPad Software, Boston, MA, USA).

5.9. Modeling of oxygen distribution in microwell-cultured pseudoislets

A model of three islets captured in a microwell array was created in COMSOL Multiphysics 6.2 (COMSOL, Inc., Burlington, MA, USA). A model geometry based on the designed arrays of variable diameters and inter-well spacing was chosen to fit the dimensions of the islet culture environment. The media column on top of the islets was set to a height of 5 mm, whereas the PDMS membrane beneath the microwell array was 400 μm thick. A symmetry condition was placed on the vertical axis on both sides of the three microwells. Islets were defined as areas where oxygen consumption R_{O_2} takes place and modeled as a Michaelis-Menten reaction (equation (1)), as previously described [66],

$$R_{O_2} = R_{\mathrm{Max},\,O_2}\,\frac{c_{O_2}}{c_{O_2} + C_{\mathrm{MM},\,O_2}} * \delta\left(c_{O_2} > C_{\mathrm{cr}}\right) \quad (1)$$

where $R_{\mathrm{Max},\,O_2} = 0.034$ mol m^{-3} s^{-1} is the highest rate at which oxygen can be consumed under optimal conditions, and $C_{\mathrm{MM},O_2} = 0.034$ mol m^{-3} is the Michaelis–Menten constant, and the oxygen concentration c_{O_2} at which the consumption rate drops to half of its maximum value. $\delta(c_{O_2} > C_{\mathrm{cr}})$ defines a Heaviside function to model the abrupt cessation of oxygen consumption in regions where the

oxygen falls below the critical concentration, where $C_{cr} = 0.0001$ mol m^{-3}, which denotes the threshold oxygen concentration below which tissue necrosis is likely to occur if exposure is prolonged, according to a previously published model [66]. The oxygen tension at the PDMS-air and culture medium-air boundaries was set to 0.20088 mol m^{-3}. The islet size was set to 100 µm, which is comparable to the average pseudoislet size in the experimental condition. The Diffusivity coefficient (D_{eff}) of the medium, PDMS, and tissue were assumed to be $D_{eff, media} = 3\ 10^{-9}$ m^2 s^{-1}, $D_{eff, PDMS} = 3.4\ 10^{-9}$ m^2 s^{-1} and $D_{eff, tissue} = 2\ 10^{-9}$ m^2 s^{-1} based on previously reported values [66, 78]. The simulation was started under normoxia and continued until equilibrium was reached.

Acknowledgment

This work was supported in part by Deutsche Forschungsgemeinschaft (DFG, German Research Foundation) (Project number 213602983—TRR 127, Project number 288034826—IRTG 2251). The authors acknowledge the excellent statistical advice provided by Dr Friedemann Uschner (Institute for Medical Informatics and Biometry, TU Dresden). This work was conducted in collaboration with the Microstructure Core Facility, a joint facility of the Technology Platform at the Center for Molecular and Cellular Bioengineering, and the Cluster of Excellence Physics of Life at TU Dresden. The core facility is supported by the Deutsche Forschungsgemeinschaft (DFG, German Research Foundation) under Germany's Excellence Strategy—EXC-2068–390729961—Cluster of Excellence Physics of Life at TU Dresden.

Data availability statement

All data that support the findings of this study are included within the article (and any supplementary files).

Supplementary data 1 available at: https://doi.org/10.1088/1748-605X/ae88a4/data1.

Conflict of interest

Authors (C. Heller, B. Ludwig, P. B. Welzel, C. Werner, S. R. Bornstein) declare that they have applied a patent concerning a macroencapsulation device and its applications (WO 2023 117 849 A1, Modular implantable device for the macroencapsulation of cells, publication date: 29.06.2023).

All authors declare no conflict of interest.

Ethical statement

No patients were investigated in this study. All animal studies were conducted with the approval of the local animal care committee (Saxony, Germany) in accordance with institutional guidelines and national animal welfare legislation (license numbers TV T 2/2018 and TV T 4/2023).

Declaration of generative AI and AI-assisted technologies in the writing process

During the preparation of this work the authors used ChatGPT, DeepL Write, and Paperpal in order to improve the readability and language of the manuscript. After using this tool/service, the authors reviewed and edited the content as needed and take full responsibility for the content of the publication.

Author contributions

Charline Rosenberger 0009-0003-0668-7157
Data curation (lead), Formal analysis (lead), Investigation (lead), Methodology (equal), Validation (lead), Visualization (lead), Writing – original draft (lead), Writing – review & editing (lead)

Carolin Heller 0000-0002-1015-675X
Conceptualization (lead), Data curation (equal), Formal analysis (equal), Investigation (equal), Methodology (equal), Project administration (lead), Resources (equal), Supervision (lead), Validation (equal), Visualization (equal), Writing – review & editing (lead)

Tomasz M Basiewicz 0009-0009-5223-0709
Formal analysis (supporting), Investigation (equal), Methodology (lead), Resources (equal), Validation (equal), Writing – review & editing (equal)

Susann Lehmann 0009-0001-0580-4580
Writing – review & editing (equal)

Victoria Sarangova
Methodology (supporting), Writing – review & editing (equal)

Hany Abdelgawad 0000-0002-9134-6167
Writing – review & editing (equal)

Undine Schubert 0000-0001-7956-2177
Writing – review & editing (equal)

Janine Schmid
Writing – review & editing (equal)

Carsten Werner 0000-0003-0189-3448
Resources (equal)

Stefan R Bornstein
Funding acquisition (equal), Resources (equal)

Petra B Welzel 0000-0002-8174-7688
Funding acquisition (equal), Supervision (equal), Writing – review & editing (equal)

Barbara Ludwig 0000-0003-0771-5247
Funding acquisition (equal), Resources (equal), Supervision (equal), Writing – review & editing (equal)

References

[1] Abadpour S, Wang C, Niemi E M and Scholz H 2021 Tissue engineering strategies for improving beta cell transplantation outcome *Curr. Transplant. Rep.* **8** 205–19
[2] Desai T A and Tang Q 2018 Islet encapsulation therapy—racing towards the finish line? *Nat. Rev. Endocrinol.* **14** 630–2
[3] Desai T and Shea L D 2017 Advances in islet encapsulation technologies *Nat. Rev. Drug Discov.* **16** 338–50
[4] Ludwig B, Heller C, Sarangova V and Welzel P B 2023 Islet macroencapsulation: strategies to boost islet graft oxygenation *Pluripotent Stem Cell Therapy for Diabetes* ed L Piemonti, J Odorico, T J Kieffer, V Sordi and E De Koning (Springer) pp 251–80
[5] Ernst A U *et al* 2022 A predictive computational platform for optimizing the design of bioartificial pancreas devices *Nat. Commun.* **13** 6031
[6] Kumagai-Braesch M, Jacobson S, Mori H, Jia X, Takahashi T, Wernerson A, Flodström-Tullberg M and Tibell A 2013 The TheraCyte^{tm} device protects against islet allograft rejection in immunized hosts *Cell Transplant.* **22** 1137–46
[7] Storrs R, Dorian R, King S R, Lakey J and Rilo H 2001 Preclinical development of the Islet Sheet *Ann. N. Y. Acad. Sci.* **944** 252–66
[8] Ludwig B *et al* 2010 A novel device for islet transplantation providing immune protection and oxygen supply *Horm. Metab. Res.* **42** 918–22
[9] Chendke G S, Kharbikar B N, Ashe S, Faleo G, Sneddon J B, Tang Q, Hebrok M and Desai T A 2023 Replenishable prevascularized cell encapsulation devices increase graft survival and function in the subcutaneous space *Bioeng. Transl. Med.* **8** e10520
[10] ViaCyte 2022 *A prospective, multicenter, open-label, first-in-human phase 1/2 study with two cohorts to evaluate the safety, tolerability, and efficacy of various doses of VC-01^{TM} combination product in subjects with type 1 diabetes mellitus clinicaltrials.gov*
[11] Jiang L, Liu J, Wang K, Gu X and Luo Y 2014 Investigating design principles of micropatterned encapsulation systems containing high-density microtissue arrays *Sci. China Life Sci.* **57** 221–31
[12] Skrzypek K, Groot Nibbelink M, Van Lente J, Buitinga M, Engelse M A, De Koning E J P, Karperien M, Van Apeldoorn A and Stamatialis D 2017 Pancreatic islet macroencapsulation using microwell porous membranes *Sci. Rep.* **7** 9186
[13] Skrzypek K, Nibbelink M G, Karbaat L P, Karperien M, Van Apeldoorn A and Stamatialis D 2018 An important step towards a prevascularized islet macroencapsulation device—effect of micropatterned membranes on development of endothelial cell network *J. Mater. Sci., Mater. Med.* **29** 91
[14] Smink A M, Skrzypek K, Liefers-Visser J A L, Kuwabara R, De Haan B J, De Vos P and Stamatialis D 2021 In vivo vascularization and islet function in a microwell device for pancreatic islet transplantation *Biomed. Mater.* **16** 035036
[15] Lee G, Jun Y, Jang H, Yoon J, Lee J, Hong M, Chung S, Kim D-H and Lee S 2018 Enhanced oxygen permeability in membrane-bottomed concave microwells for the formation of pancreatic islet spheroids *Acta Biomater.* **65** 185–96
[16] Zbinden A *et al* 2020 Fluorescence lifetime metabolic mapping of hypoxia-induced damage in pancreatic pseudo-islets *J. Biophotonics* **13** e202000375
[17] Giuliani M, Moritz W, Bodmer E, Dindo D, Kugelmeier P, Lehmann R, Gassmann M, Groscurth P and Weber M 2005 Central necrosis in isolated hypoxic human pancreatic islets: evidence for postisolation ischemia *Cell Transplant.* **14** 67–76
[18] Komatsu H, Kandeel F and Mullen Y 2018 Impact of oxygen on pancreatic islet survival *Pancreas* **47** 533–43
[19] Lehmann R, Zuellig R A, Kugelmeier P, Baenninger P B, Moritz W, Perren A, Clavien P-A, Weber M and Spinas G A 2007 Superiority of small islets in human islet transplantation *Diabetes* **56** 594–603
[20] Selimović Š, Piraino F, Bae H, Rasponi M, Redaelli A and Khademhosseini A 2011 Microfabricated polyester conical microwells for cell culture applications *Lab Chip* **11** 2325
[21] Mohr J C, Zhang J, Azarin S M, Soerens A G, De Pablo J J, Thomson J A, Lyons G E, Palecek S P and Kamp T J 2010 The microwell control of embryoid body size in order to regulate cardiac differentiation of human embryonic stem cells *Biomaterials* **31** 1885–93
[22] Karp J M *et al* 2007 Controlling size, shape and homogeneity of embryoid bodies using poly(ethylene glycol) microwells *Lab Chip* **7** 786
[23] Bernard A B, Lin C-C and Anseth K S 2012 A microwell cell culture platform for the aggregation of pancreatic β-cells *Tissue Eng. C* **18** 583–92
[24] Yeon S-E, No D Y, Lee S-H, Nam S W, Oh I-H, Lee J, Kuh H-J and Munshi H G 2013 Application of concave microwells to pancreatic tumor spheroids enabling anticancer drug evaluation in a clinically relevant drug resistance model *PLoS One* **8** e73345
[25] Myrick R J *et al* 2023 Micropyramid-patterned, oxygen-permeable bottomed dish for high density culture of pancreatic islets *Biofabrication* **15** 015018
[26] Hilderink J, Spijker S, Carlotti F, Lange L, Engelse M, van Blitterswijk C, de Koning E, Karperien M and van Apeldoorn A 2015 Controlled aggregation of primary human pancreatic islet cells leads to glucose-responsive pseudoislets comparable to native islets *J. Cell. Mol. Med.* **19** 1836–46
[27] Buitinga M *et al* 2017 Micro-fabricated scaffolds lead to efficient remission of diabetes in mice *Biomaterials* **135** 10–22
[28] Hadavi E, De Vries R H W, Smink A M, De Haan B, Leijten J, Schwab L W, Karperien M H B J, De Vos P, Dijkstra P J and van Apeldoorn A A 2021 Van Apeldoorn AA 2021 *In vitro* degradation profiles and in vivo biomaterial–tissue interactions of microwell array delivery devices *J. Biomed. Mater. Res. B* **109** 117–27
[29] Myasnikova D, Osaki T, Onishi K, Kageyama T, Zhang molino B and Fukuda J 2019 Synergic effects of oxygen supply and antioxidants on pancreatic β-cell spheroids *Sci. Rep.* **9** 1802
[30] Hwang J W, Lee B R, Jung M J, Jung H S, Hwang Y H, Kim M J, Lee S H and Lee D Y 2011 Functional clustering of pancreatic islet cells using concave microwell array *Macromol. Res.* **19** 1320–6
[31] Tanyeri M and Tay S 2018 Viable cell culture in PDMS-based microfluidic devices, *in Methods in Cell Biology* vol 148 (Elsevier) pp 3–33
[32] Rezai P, Wu W-I and Selvaganapathy P R 2012 Microfabrication of polymers for bioMEMS *MEMS for Biomedical Applications* (Elsevier) pp 3–45
[33] Olmos C M *et al* 2020 Cost-effective fabrication of photopolymer molds with multi-level microstructures for PDMS microfluidic device manufacture *RSC Adv.* **10** 4071–9

[34] Simmons A, Padsalgikar A D, Ferris L M and Poole-warren L A 2008 Biostability and biological performance of a PDMS-based polyurethane for controlled drug release *Biomaterials* **29** 2987–95
[35] Hassler C, Boretius T and Stieglitz T 2011 Polymers for neural implants: polymers for neural implants *J. Polym. Sci. B* **49** 18–33
[36] Borenstein J T 2008 Tissue engineering *Comprehensive Microsystems* (Elsevier) pp 541–83
[37] Pinho D, Muñoz-sánchez B N, Anes C F, Vega E J and Lima R 2019 Flexible PDMS microparticles to mimic RBCs in blood particulate analogue fluids *Mech. Res. Commun.* **100** 103399
[38] Shi Y, Hu M, Xing Y and Li Y 2020 Temperature-dependent thermal and mechanical properties of flexible functional PDMS/paraffin composites *Mater. Des.* **185** 108219
[39] Amjadi M, Pichitpajongkit A, Lee S, Ryu S and Park I 2014 Highly stretchable and sensitive strain sensor based on silver nanowire–elastomer nanocomposite *ACS Nano* **8** 5154–63
[40] Gohil S V, Suhail S, Rose J, Vella T and Nair L S 2017 Polymers and composites for orthopedic applications *Materials for Bone Disorders* (Elsevier) pp 349–403
[41] Salazar-Hernández C, Salazar-Hernández M, Carrera-cerritos R, Mendoza-miranda J M, Elorza-rodríguez E, Miranda-avilés R and Mocada-sánchez C D 2019 Anticorrosive properties of PDMS-Silica coatings: effect of methyl, phenyl and amino groups *Prog. Org. Coat.* **136** 105220
[42] Ariati R, Sales F, Souza A, Lima R A and Ribeiro J 2021 Polydimethylsiloxane composites characterization and its applications: a review *Polymers* **13** 4258
[43] Akther F, Yakob S B, Nguyen N-T and Ta H T 2020 Surface modification techniques for endothelial cell seeding in PDMS microfluidic devices *Biosensors* **10** 182
[44] Gokaltun A, Yarmush M L, Asatekin A and Usta O B 2017 Recent advances in nonbiofouling PDMS surface modification strategies applicable to microfluidic technology *Technology* **05** 1–12
[45] Azizipour N, Avazpour R, Sawan M, Rosenzweig D H and Ajji A 2022 Uniformity of spheroid-on-chip by surface treatment of PDMS microfluidic platforms *Sens. Diagn.* **1** 750–64
[46] Wu Z and Hjort K 2009 Surface modification of PDMS by gradient-induced migration of embedded Pluronic *Lab Chip* **9** 1500
[47] Guo W, Chen Z, Feng Z, Li H, Zhang M, Zhang H and Cui X 2022 Fabrication of concave microwells and their applications in micro-tissue engineering: a review *Micromachines* **13** 1555
[48] Qin D, Xia Y and Whitesides G M 2010 Soft lithography for micro- and nanoscale patterning *Nat. Protoc.* **5** 491–502
[49] Zhang L-G, Zhong D-H, Zhang Y, Li C-Z, Kisaalita W S and Wu Z-Z 2014 A microwell pattern for C17.2 cell aggregate formation with concave cylindrical surface induced cell peeling *Biomaterials* **35** 9423–37
[50] Essaouiba A, Okitsu T, Jellali R, Shinohara M, Danoy M, Tauran Y, Legallais C, Sakai Y and Leclerc E 2020 Microwell-based pancreas-on-chip model enhances genes expression and functionality of rat islets of Langerhans *Mol. Cell. Endocrinol.* **514** 110892
[51] Stell A, Vaithilingam V, Mohammed S G, De Vries R H W, De Bont D F A, De Koning E J P and Van Apeldoorn A A 2025 A hybrid implant combining a macroporous device with immunoprotective microcapsules for cell therapy applications: a conceptual *in vitro* study *Mater. Today Bio* **31** 101574
[52] Buitinga M, Truckenmüller R, Engelse M A, Moroni L, Ten Hoopen H W M, Van Blitterswijk C A, De Koning E J P, Van Apeldoorn A A and Karperien M 2013 Microwell scaffolds for the extrahepatic transplantation of islets of Langerhans *PLoS One* **8** e64772
[53] Rojas-Canales D M *et al* 2018 Oxygen-permeable microwell device maintains islet mass and integrity during shipping *Endocr. Connect.* **7** 490–503
[54] Pham C H L, Zuo Y, Chen Y, Tran N M, Nguyen D T and Dang T T 2023 Waffle-inspired hydrogel-based macrodevice for spatially controlled distribution of encapsulated therapeutic microtissues and pro-angiogenic endothelial cells *Bioeng. Transl. Med.* **8** e10495
[55] Kato H *et al* 2022 Microwell culture platform maintains viability and mass of human pancreatic islets *Front. Endocrinol.* **13** 1015063
[56] Shinohara M, Kimura H, Montagne K, Komori K, Fujii T and Sakai Y 2014 Combination of microwell structures and direct oxygenation enables efficient and size-regulated aggregate formation of an insulin-secreting pancreatic β-cell line *Biotechnol. Prog.* **30** 178–87
[57] Smink A M *et al* 2016 Selection of polymers for application in scaffolds applicable for human pancreatic islet transplantation *Biomed. Mater.* **11** 035006
[58] Tsuda Y, Kato-negishi M, Okitsu T and Takeuchi S 2009 Size-controlled islet-cell spheroids for geometric analysis of insulin secretion *2009 IEEE 22nd Int. Conf. on Micro Electro Mechanical Systems* (IEEE) pp 423–6
[59] Kusamori K, Nishikawa M, Mizuno N, Nishikawa T, Masuzawa A, Shimizu K, Konishi S, Takahashi Y and Takakura Y 2014 Transplantation of insulin-secreting multicellular spheroids for the treatment of type 1 diabetes in mice *J. Control. Release* **173** 119–24
[60] Carter S-S D, Atif A-R, Kadekar S, Lanekoff I, Engqvist H, Varghese O P, Tenje M and Mestres G 2020 PDMS leaching and its implications for on-chip studies focusing on bone regeneration applications *Organs-on-a-Chip* **2** 100004
[61] Zhang S and Staples A E 2025 Effects of natural aging on hydrophilicity and mechanical properties of PDMS in various storage environments *npj Mater. Degrad.* **9** 109
[62] Jun Y, Kang A R, Lee J S, Jeong G S, Ju J, Lee D Y and Lee S-H 2013 3D co-culturing model of primary pancreatic islets and hepatocytes in hybrid spheroid to overcome pancreatic cell shortage *Biomaterials* **34** 3784–94
[63] Mouré A *et al* 2022 Optimization of an O_2-balanced bioartificial pancreas for type 1 diabetes using statistical design of experiment *Sci. Rep.* **12** 4681
[64] Wenger R, Kurtcuoglu V, Scholz C, Marti H and Hoogewijs D 2015 Frequently asked questions in hypoxia research *Hypoxia* **35** 35–43
[65] Castro D, Patil S M, Zubair M and Keenaghan M 2024 Arterial blood gas *StatPearls* (StatPearls Publishing) (available at: https://www.ncbi.nlm.nih.gov/books/NBK536919/)
[66] Buchwald P 2009 FEM-based oxygen consumption and cell viability models for avascular pancreatic islets *Theor. Biol. Med. Model.* **6** 5
[67] Avgoustiniatos E S *et al* 2024 Silicone rubber membrane devices permit islet culture at high density without adverse effects *Front. Bioeng. Biotechnol.* **12** 1401608
[68] Patel S N, Ishahak M, Chaimov D, Velraj A, LaShoto D, Hagan D W, Buchwald P, Phelps E A, Agarwal A and Stabler C L 2021 Organoid microphysiological system preserves pancreatic islet function within 3D matrix *Sci. Adv.* **7** eaba5515
[69] Olsson R and Carlsson P-O 2011 A low-oxygenated subpopulation of pancreatic islets constitutes a functional reserve of endocrine cells *Diabetes* **60** 2068–75
[70] Carlsson P O, Liss P, Andersson A and Jansson L 1998 Measurements of oxygen tension in native and transplanted rat pancreatic islets *Diabetes* **47** 1027–32
[71] Shi Y, Ma J, Zhang X, Li H, Jiang L and Qin J 2015 Hypoxia combined with spheroid culture improves cartilage specific function in chondrocytes *Integr. Biol.* **7** 289–97

[72] Tan J Y, Goh G and Kim J 2020 Microfabrication of microlens by timed-development-and-thermal-reflow (TDTR) process for projection lithography *Micromachines* **11** 277
[73] Munief W-M, Heib F, Hempel F, Lu X, Schwartz M, Pachauri V, Hempelmann R, Schmitt M and Ingebrandt S 2018 Silane deposition via gas-phase evaporation and high-resolution surface characterization of the ultrathin siloxane coatings *Langmuir* **34** 10217–29
[74] Heller C 2024 PDMS microwell array cell culture insert for 24-well plate (https://doi.org/10.5281/zenodo.13944310)
[75] Carter J D, Dula S B, Corbin K L, Wu R and Nunemaker C S 2009 A practical guide to rodent islet isolation and assessment *Biol. Proced. Online* **11** 3
[76] Lakens D 2017 Equivalence tests: a practical primer for *t* tests, correlations, and meta-analyses *Soc. Psychol. Pers. Sci.* **8** 355–62
[77] Caldwell A R 2022 Exploring equivalence testing with the updated TOSTER R package (https://doi.org/10.31234/osf.io/ty8de)
[78] Merkel T C, Bondar V I, Nagai K, Freeman B D and Pinnau I 2000 Gas sorption, diffusion, and permeation in poly(dimethylsiloxane) *J. Polym. Sci. B* **38** 415–34